Characterization of a steam plasma jet at atmospheric pressure

2012 Plasma Sources Sci. Technol. 21 015009

(http://iopscience.iop.org/0963-0252/21/1/015009)

IOP PUBLISHING PLASMA SOURCES SCIENCE AND TECHNOLOGY

Plasma Sources Sci. Technol. **21** (2012) 015009 (12pp) doi:10.1088/0963-0252/21/1/015009

Characterization of a steam plasma jet at atmospheric pressure

Guohua Ni[1], Peng Zhao[1], Cheng Cheng[1], Ye Song[1], Hirotaka Toyoda[2] and Yuedong Meng[1]

[1] Institute of Plasma Physics, Chinese Academy of Sciences, Hefei 230031, People's Republic of China
[2] Department of Electrical Engineering and Computer Science, Nagoya University, Nagoya, Japan

E-mail: ghni@ipp.ac.cn

Received 3 July 2011, in final form 5 December 2011
Published 31 January 2012
Online at stacks.iop.org/PSST/21/015009

Abstract
An atmospheric steam plasma jet generated by an original dc water plasma torch is investigated using electrical and spectroscopic techniques. Because it directly uses the water used for cooling electrodes as the plasma-forming gas, the water plasma torch has high thermal efficiency and a compact structure. The operational features of the water plasma torch and the generation of the steam plasma jet are analyzed based on the temporal evolution of voltage, current and steam pressure in the arc chamber. The influence of the output characteristics of the power source, the fluctuation of the arc and current intensity on the unsteadiness of the steam plasma jet is studied. The restrike mode is identified as the fluctuation characteristic of the steam arc, which contributes significantly to the instabilities of the steam plasma jet. In addition, the emission spectroscopic technique is employed to diagnose the steam plasma. The axial distributions of plasma parameters in the steam plasma jet, such as gas temperature, excitation temperature and electron number density, are determined by the diatomic molecule OH fitting method, Boltzmann slope method and H_β Stark broadening, respectively. The steam plasma jet at atmospheric pressure is found to be close to the local thermodynamic equilibrium (LTE) state by comparing the measured electron density with the threshold value of electron density for the LTE state. Moreover, based on the assumption of LTE, the axial distributions of reactive species in the steam plasma jet are estimated, which indicates that the steam plasma has high chemical activity.

(Some figures may appear in colour only in the online journal)

1. Introduction

Thermal plasmas are widely used in materials and manufacturing industries [1–5] (cutting, welding, spraying, plasma synthesis, chemical vapor deposition (CVD) and metallurgy) and environmental industry [6–15] (Municipal solid waste incinerator fly ash treatment, harmful industrial waste pyrolysis and solidification, radioactive waste reduction and vitrification, coal gasification) because of their high temperature and high energy density. Among the various thermal plasmas, steam thermal plasmas have the distinctive features of high enthalpy and high oxidation–reduction capacity, and they are also environmentally friendly. These features make them suitable for applications in the fields of environment, energy and materials, such as hazardous waste treatment, solid fuel gasification and plasma spraying. Kim *et al* [16] studied the performance of a steam plasma system for PCB (polychlorinated biphenyls) waste treatment, and confirmed that the steam plasma process for converting hazardous waste to energy is more effective than the air plasma process and the conventional incineration process. Nishikawa *et al* [17] investigated the effect of a dc steam plasma on gasifying carbonized waste, and found that the steam plasma is much more effective in reducing the weight of carbonaceous wastes and producing high concentrations of H_2 and CO compared with the cases of Ar plasma. For many years, water-stabilized plasma systems have been commercially used successfully for plasma spraying. Compared with the commonly used gas-stabilized torches, they have a high power throughput, because of their high outlet velocities, temperature and plasma enthalpy [18].

The steam thermal plasma sources commonly used in these processes are dc hybrid stabilized plasma torches, which generally use a mixture of gas (i.e. argon, nitrogen or air)

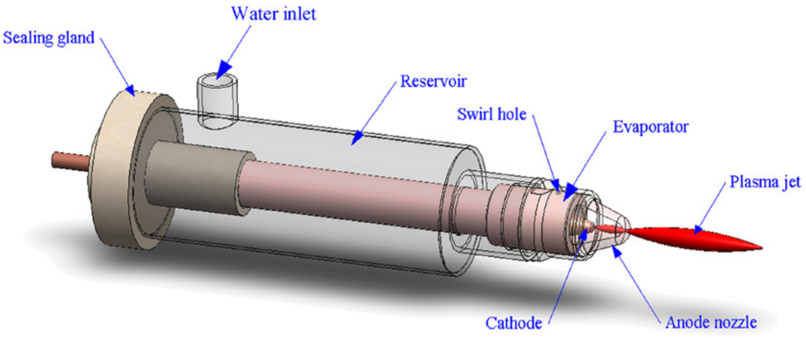

Figure 1. Configuration of the dc water plasma torch.

and water as the plasma-supporting gas. However, the lower thermal efficiency of these torches (because a large amount of energy is taken away by the water used for cooling the electrodes) limits their industrial application. For this reason, a novel water plasma torch was introduced due to its higher efficiency [19]. Moreover, it is necessary to understand the characteristics of a steam plasma jet, including the basic plasma phenomena, which will improve the performance of the torch, further develop steam thermal plasma technology and enhance its potential industrial applications.

In this study, an original dc water plasma torch producing a 100% steam plasma jet is created for the purposes of organic waste treatment. The operational feature of the torch is investigated by virtual instrument technology. The high thermal efficiency of the device and high enthalpy of the steam thermal plasma are tested by experiment and calculation. The output characteristics of the power source, the fluctuation of the arc and current intensity impact on the fluctuation of the steam plasma jet are investigated and analyzed by means of the fast Fourier transform (FFT) method. The optical emission spectroscopic (OES) technique is employed to diagnose the key parameters of the water plasma by recording and analyzing the water plasma spectra along the jet axis. The gas temperatures of the water plasma are determined by hydroxyl rotational temperature, obtained by comparing the synthetic hydroxyl spectrum with the measured one. The excitation temperatures of the water plasma are calculated using the Boltzmann plot method, and the electron number densities are derived from the Stark broadening of H_β. In addition, criteria of local thermodynamic equilibrium (LTE) are fulfilled by the water plasma and the distributions of chemical compositions in the plasma jet are investigated.

2. Experimental

2.1. Plasma source

The configuration of the dc water plasma torch used in our experiment is shown in figure 1. Compared with a conventional plasma torch, this one has a distinctive design with 100% steam as the plasma-forming gas. A felt in a reservoir is used to store water, in order to cool the electrodes and provide the plasma-working gas. The water is injected into the reservoir from the water inlet and its flow rate is controlled by a peristaltic pump. The plasma is created as follows: an arc is initiated between a zirconium cathode of diameter 2 mm embedded into a copper rod and a nozzle-type anode of copper. Then heat energy is released by the arc on the nozzle and the evaporator evaporates the water held in the reservoir. The resultant steam passes through the swirl hole in the evaporator and enters the arc chamber as vortex gas. With an increase in the amount of steam, a steam plasma jet is formed at the exit of the nozzle. Thus, the torch can work in high-efficiency mode because water cools the electrode and acts as the plasma-forming gas at the same time. The consumption of water is approximately 3 ml min^{-1} at an arc power of 1 kW. The torch is supplied by IGBT constant current power sources, with a maximum voltage output of 350 V. The output current (0–10 A) can be adjusted by a current regulator.

In a previous study [19], we found that the temperature of the shell of the torch body is very high after the torch has worked for a long time, i.e. an hour, which affects the stability of the water plasma operation. The detailed reason will be described in the following. In view of this state, a water cooling equipment is used for maintaining the shell's temperature constant. Figure 2 shows the water-cooling equipment modification of the torch body.

2.2. The measurement system

A virtual instrument and spectroscopic diagnostic technology are used for diagnosis and analysis of the characteristics of the steam plasma jet. Figure 3 shows a schematic diagram of the experimental set-up used for this purpose, including the following parts: water plasma torch, dc power supply, water supply system, virtual instrument testing circuit and spectrum diagnostic system. In addition, three thermocouples are used to measure the water temperature at the inlet and outlet of the cooling circuits and the temperature of the anode outer surface, respectively.

The virtual instrument circuit comprises a signal conditioning circuit, data acquisition program module and personal computer. NI Cdaq-9174 and NI 9222 are used for construction of NI CompactDAQ systems, which are composed of a virtual instrument hardware module for signal acquisition. NI Cdaq-9174 is a four-slot NI CompactDAQ chassis designed for small, portable, mixed-measurement test systems. NI 9222 is a high-speed, simultaneous analog input module with the following characteristics: four differential channels, software selectable gain, 16 bits resolution with

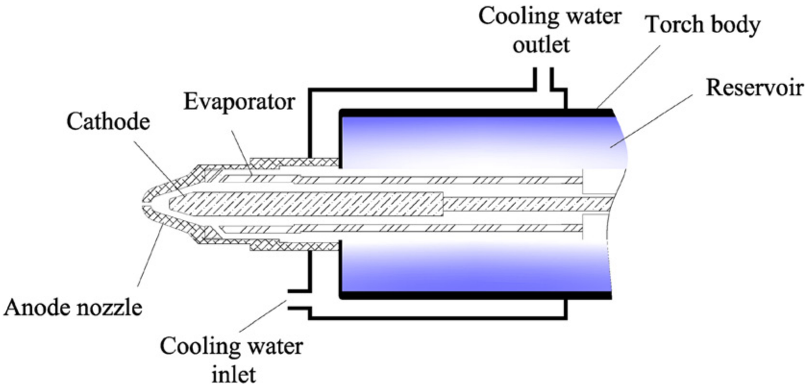

Figure 2. Water-cooling equipment modification to the torch body.

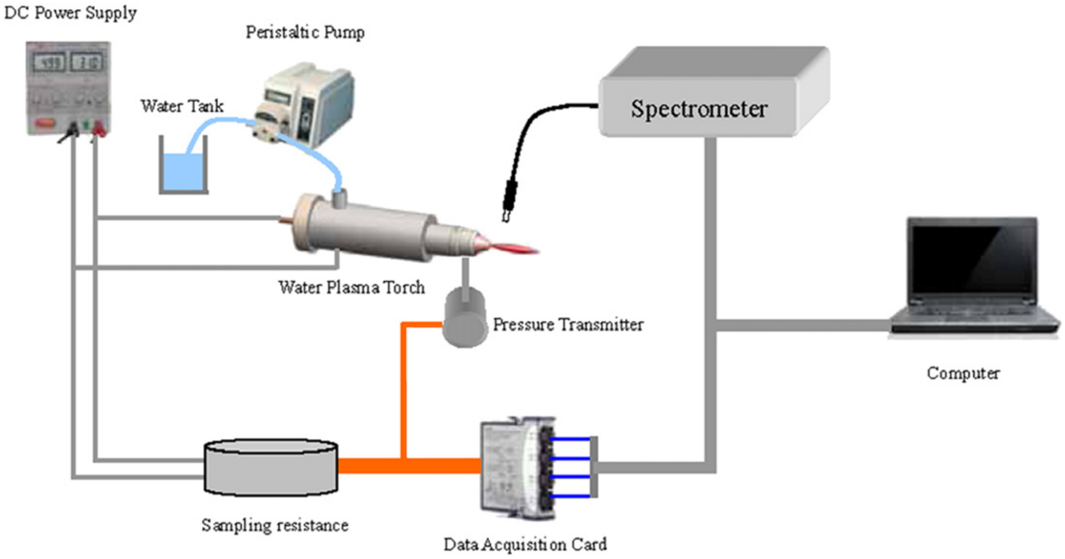

Figure 3. Schematic diagram of the experimental set-up.

a sampling rate of 500 kS s^{-1}. Three A/D channels are used, which are connected to the circuit through signal acquisition and conditioning circuits, to acquire and adjust the measured voltages to the A/D card ranges. One signal acquisition circuit is connected in parallel to the discharge circuit through a sampling resistance of 1 kΩ in a resistance voltage divider to acquire the arc voltage signal. Another one is connected in series to the discharge circuit through a sampling resistance of 0.5 Ω to acquire the arc current signal. The last one is connected to the output of a high-temperature pressure transmitter (PT421) to acquire the pressure signal. In order to measure the pressure in the arc chamber of the water torch during its operation, one nozzle is modified for pressure measurements inside the arc chamber, as shown in figure 4.

In order to compare the emission spectra along the plasma jet, a VUV silica optical fiber is placed downstream at various distances from the nozzle exit (0 mm $\leqslant z \leqslant$ 80 mm). The optical fiber is connected to a AvaSpec-1024 spectrometer with a spectral resolution of 0.07 nm covering the spectral range 200–1050 nm. The spectrum of the discharge region is obtained from integrated light by looking directly into the plasma vertically.

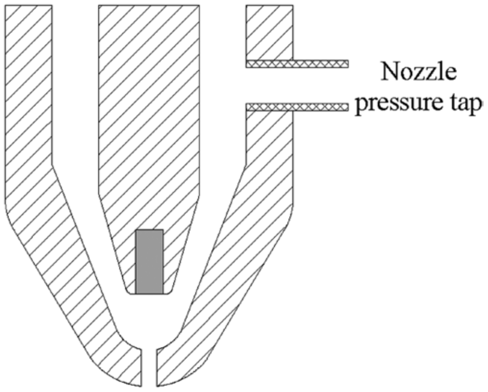

Figure 4. Pressure tap modification to the nozzle.

3. Results and discussion

3.1. Operational feature

In general, a gas-stabilized torch can soon reach a stable working condition. In our plasma torch, due to the fact that liquid water is used directly as the plasma-forming gas, it will take some time to complete the water phase change and cause

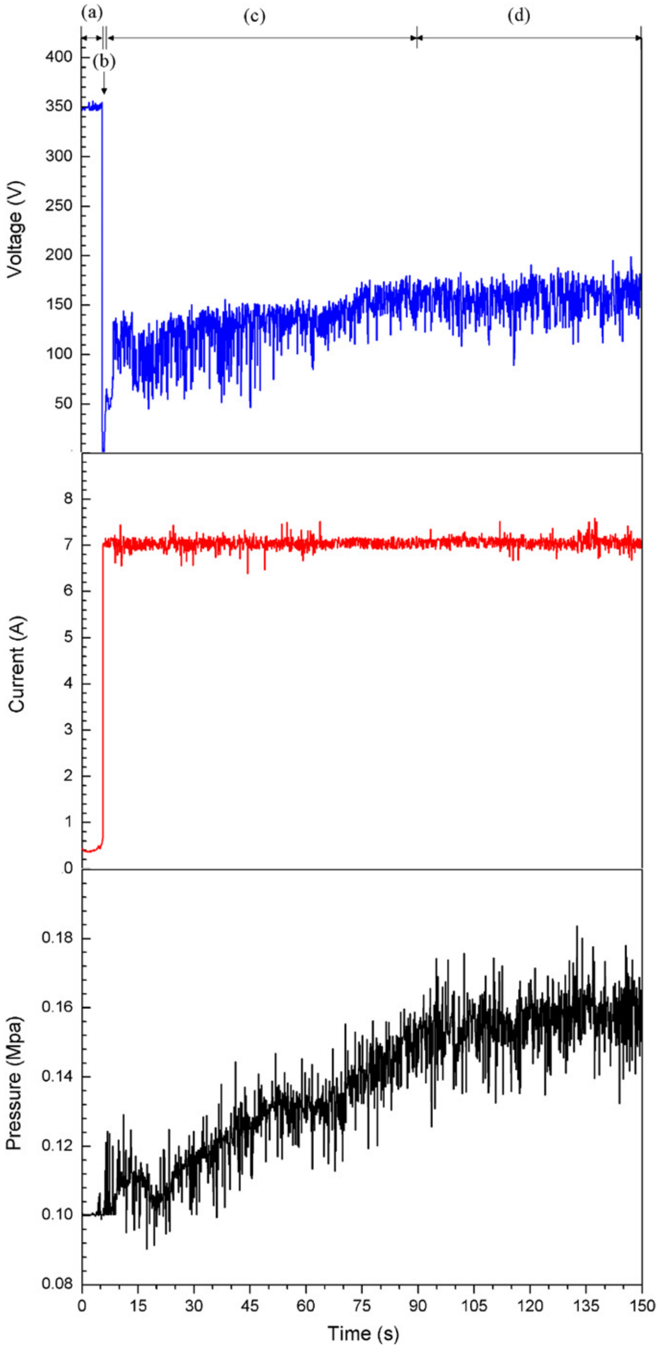

Figure 5. Temporal evolution of the torch parameters (arc voltage, arc current and pressure) from the beginning to the stable working state of the torch, under the experimental conditions of 7 A current, and a distance of 5 mm between the cathode and the anode: (a) before discharge; (b) at the time when the cathode comes into contact with the anode; (c) when the amount of steam increases; (d) when the amount of steam is stabilized.

the water vapor pressure to reach a stable state. Figure 5 shows the temporal evolution of the torch parameters (arc voltage, arc current and pressure) from the beginning to the stable working state of the torch, under the experimental conditions of 7 A current, and a distance of 5 mm between the cathode and the anode.

At the beginning, the presence of liquid water in the arc chamber cannot be broken down under the applied dc voltage, but there is a small current between the cathode and the anode, shown in region (a) of figure 5. Therefore, it can be inferred that water is heated into water vapor by Joule heating to lead to vapor–water two-phase coexistence in the arc chamber. In period (b), there is a short-circuit current because of the cathode being in contact with the anode. Once the cathode is separated from the anode, the water plasma arc is ignited, shown in region (c) of figure 5. There may be plasma–vapor–water three-phase coexistence in the arc chamber at the beginning of period (c). During this process, with the increase in heat, liquid water soon evaporates completely in the arc chamber and the steam pressure in the arc chamber gradually increases. As the pressure of steam P increases, the cross section of the arc column becomes smaller because the higher steam flow rate enhances the vortex effect so that cold steam forces the arc column to be constricted around the axis. Accordingly, the increase in arc resistance results in a rise in the arc voltage V, as shown in figure 5, region (c), therefore the power output E is also augmented, which results in the fact that heat Q is transferred to the electrodes and temperature T of the water in the reservoir is increased. In summary, the effect of heat Q is represented by a chain of causal links:

$$Q\uparrow\rightarrow T\uparrow\rightarrow P\uparrow\rightarrow V\uparrow\rightarrow E\uparrow\rightarrow Q\uparrow. \qquad (1)$$

On the basis of the above relationship, it is understandable that water-cooling equipment modification is used in our experiment to maintain the temperature of the water in the reservoir.

When thermal equilibrium is established in the torch, the arc voltage is stabilized, as shown in period (d) in figure 5, which means steam flows into the arc chamber steadily, and is then excited into a steam thermal plasma jet.

3.2. Thermal efficiency and specific enthalpy

Thermal efficiency is an important factor for a dc plasma torch, because it influences the economical aspect during its application. For a non-transferred gas-stabilized dc plasma torch, thermal efficiency η is defined as [20]

$$\eta=\frac{E_{\text{input}}-Q_{\text{cooling}}}{E_{\text{input}}}, \qquad (2)$$

where E_{input} is the power input, Q_{cooling} is the heat loss due to cooling water. For this torch, Q_{cooling} can be written as

$$Q_{\text{cooling}}=Q_{\text{rad}}+Q_{\text{conv}}+Q_{\text{cw}}, \qquad (3)$$

with Q_{rad} being the energy loss due to heat radiation by the anode surface to ambient air, Q_{conv} the energy loss due to convection between the anode surface and ambient air and Q_{cw} the energy loss due to cooling water for the torch body. Therefore, the thermal efficiency η of the torch reads

$$\begin{aligned}\eta&=\frac{E_{\text{input}}-(Q_{\text{rad}}+Q_{\text{conv}}+Q_{\text{cw}})}{E_{\text{input}}}\\&=[VI-[A\varepsilon\sigma(T_{\text{s}}^4-T_{\text{sur}}^4)\\&\quad+Ah(T_{\text{s}}-T_{\infty})+4.18c_{\text{wc}}\cdot q_{\text{wc}}(T_2-T_1)]][VI]^{-1}, \qquad (4)\end{aligned}$$

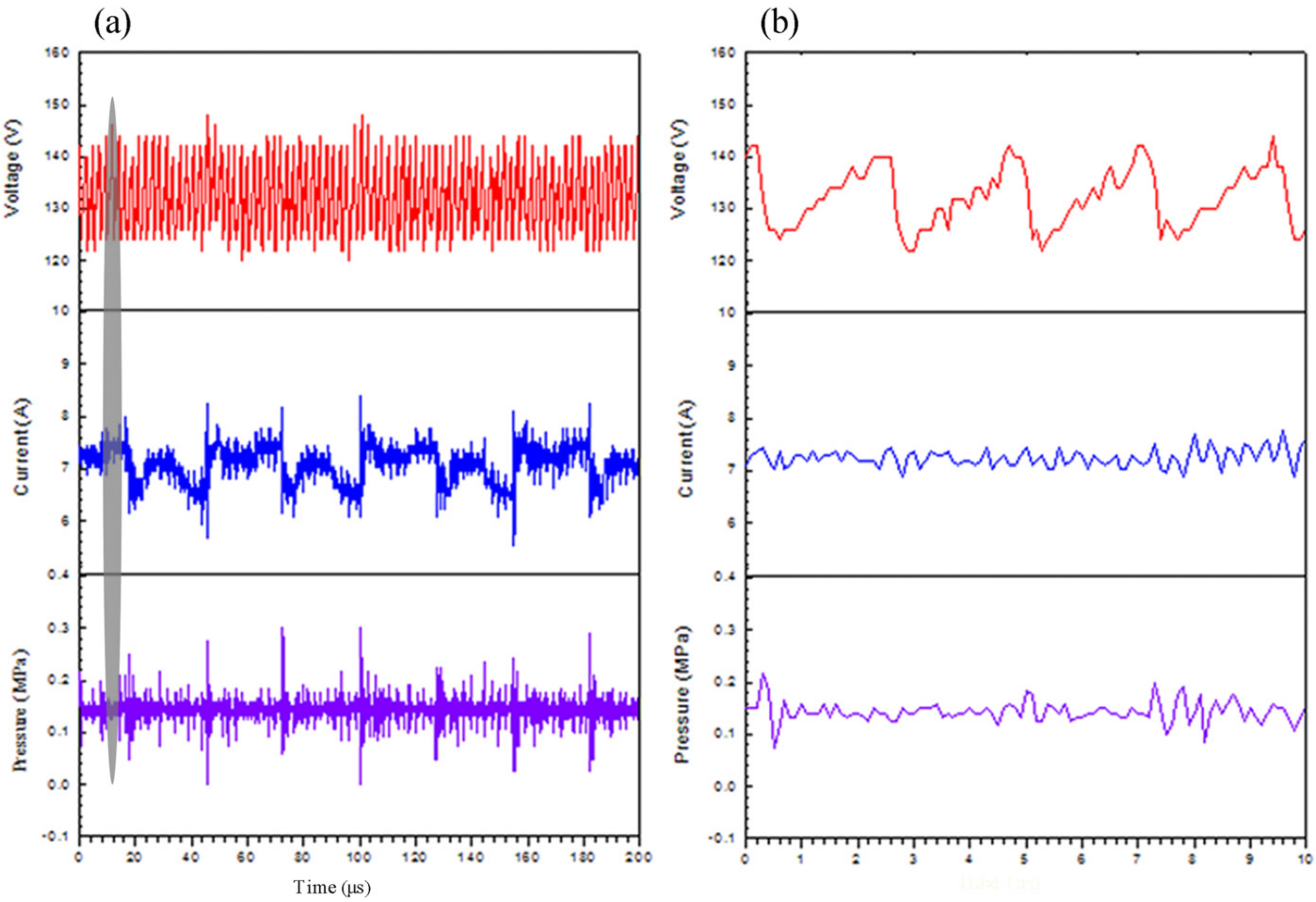

Figure 6. (*a*) Typical time-resolved arc voltage, current and pressure signal for the water torch; (*b*) time expansion of (*a*).

where V is the arc voltage, I is the arc current, A is the outer surface area of the anode, ε is the emissivity of the anode surface, σ is the Stefan–Boltzmann constant, h is the anode–environment convective heat transfer coefficient, $T_{\mathrm{sur}} = T_\infty = 300\,\mathrm{K}$ is the ambient temperature, T_{s} is the temperature of the anode outer surface, c_{wc} is the specific heat of water, q_{wc} is the volume flux of cooling water, and T_2 and T_1 are the water temperatures at the inlet and outlet, respectively. In our experiment, the thermal efficiency of the torch is approximately 90.0%. This value is much higher than those of other dc plasma torches, which is attributed to the special design of this torch as explained above.

The specific enthalpy of the plasma at the torch exit can be deduced from the energy loss due to heat radiation by the anode surface to ambient air, convection between the anode surface and ambient air and cooling water for the torch body, expressed as

$$h_{\mathrm{p}} = \frac{VI - (Q_{\mathrm{rad}} + Q_{\mathrm{conv}} + Q_{\mathrm{cw}})}{q_{\mathrm{wp}}} + h_0, \qquad (5)$$

where h_0 is the specific enthalpy of the plasma-working gas (water) before entering the plasma torch, q_{wp} is the mass flow rate of the plasma working gas (water). In equation (5), the term of kinetic energy contributing to the net power of the torch is completely neglected due to the low plasma velocity (about $100\,\mathrm{m\,s^{-1}}$) at the torch exit. Under our operating conditions (arc power about 1 kW), the specific enthalpy of the water plasma is $(18.7 \pm 1)\,\mathrm{MJ\,kg^{-1}}$, which is much higher than that of a thermal plasma using other plasma-forming gases, i.e. argon, nitrogen, air, etc, and this is confirmed by the fact that the steam thermal plasma has the characteristic of high enthalpy.

3.3. *Unsteadiness of the steam plasma jet*

The arc plasma jet is demonstrated to be unsteady, which is an important physical phenomenon and influences the performance of plasma processes [21–26], such as plasma spraying and treatment of hazardous waste. The instabilities of a plasma jet are best reflected by fluctuations of the electrical signals. Figure 6(*a*) shows the typical time-resolved electrical signal (arc voltages and current) and steam pressure in the arc chamber for the water torch. The arc voltage shows a strong fluctuation between 120 and 145 V, while the signal of the arc current has a periodicity of 55 μs, which is governed by the 18 kHz characteristic frequency of the IGBT switching of the power supply. Corresponding to the maximum fluctuation of the current at each half cycle, the pressure signal exhibits a feature of ‘surging’ and oscillation. Figure 6(*b*) is a time expansion of the highlighted region in figure 6(*a*), so that these signals (especially for the voltage signal) can be well distinguished. The arc current and steam pressure in the chamber remain constant, while an asymmetric sawtooth-like

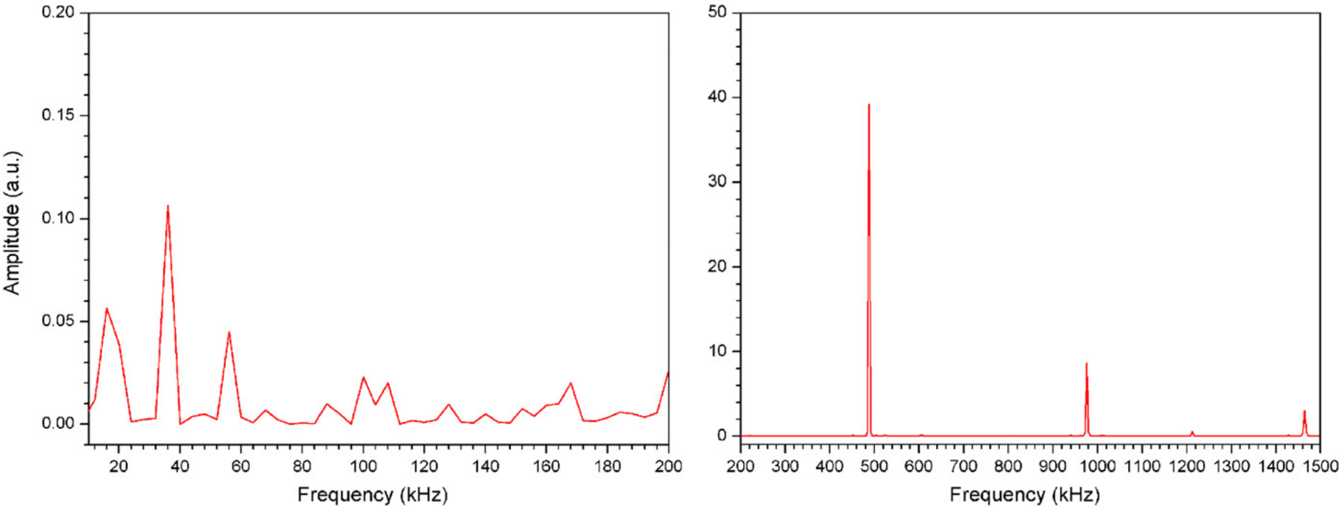

Figure 7. Voltage power spectra for the steam plasma arc, under the experimental conditions of 7 A current and 150 V arc voltage.

shape of the voltage trace, ascribed to high-frequency restrike fluctuations, is clearly observed. The arc voltage rises slowly, corresponding to the arc root displacement downstream in the flow direction, which is far away from that of the voltage decrease associated with the upstream movement of the arc root in the direction opposite to the flow. The arc voltage drops rapidly as a new current path is suddenly created by an electric breakdown [27].

Fast Fourier transform (FFT) is used to analyze the arc fluctuations and dynamic behavior of the steam plasma jet. Figure 7 shows the power spectral density against frequency spectrum for an arc current of 7 A. In all the amplitude spectra, the amplitude peaks of 490 kHz and its harmonics are the most prominent. The FFT reveals the presence of a prominent peak and its harmonics in the voltage power spectra. These frequencies are attributed to the inherent characteristics of restrike phenomena, namely the regular motion of the arc root on the wall of the arc channel.

At lower frequencies (10–200 kHz), amplitude peaks of 18 and 36 kHz, including the sum of these frequencies and their harmonics are also observed, which originated from the fluctuation of the output of the power supply, since the typical characteristic frequency of the switch mode power supply is 18 kHz. This means that the output characteristics of the power supply have an effect on the fluctuation of the steam plasma jet. However, this effect on jet fluctuation is very weak, as shown in figure 7.

The impact of arc current intensity on the voltage power spectra is clearly visible. With an increase in arc current (figure 8), the peaks in the spectra shift to higher frequencies while the amplitudes decrease. A similar phenomenon was observed by Singh *et al* and Pauvit *et al* [28, 29]. It can be interpreted by anode spot motion, which is governed by the thickness and stability of the colder water vapor layer surrounding the plasma column. The increase in arc current results in layer thinning, hence the peak frequency increases. Note that the bands around the peak are observed at high currents, i.e. 9 and 10 A. It can be interpreted that intensified turbulence of the plasma jet influences the restrike mode, in which the restrikes are more complicated than the plasma jet at low currents. Here, in addition to the regular 'upstream' restrike, 'downstream' restrike and arc-to-arc restrikes also become important causes for the fluctuation of the plasma jet.

3.4. Spectroscopic diagnostic

3.4.1. Gas temperature. The gas temperature describes the macroscopic properties of a plasma, which is an important parameter for an atmospheric steam plasma jet. Because the gas temperature is closely related to the rotational temperature of an atmospheric plasma, it can be obtained by spectroscopic methods used to measure the rotational temperature. In order to measure the axial temperature distribution of the plasma jet, the experimental data of the optical signals are obtained through an optical fiber placed near a specific portion z from the exit of the nozzle. The optical emission data of the OH spectrum used for the gas temperature calculation from the position of each portion of the plasma jet were digitalized and stored in a computer. Figure 9 shows the optical emission spectrum (OES) of the steam plasma jet at different positions ($z = 0$, 5, 15, 20 mm) downstream. The hydroxyl (OH) molecular band ($A\,^2\Sigma^+, v = 0 \rightarrow X\,^2\Pi, v' = 0$, 306–310 nm) is observed in the emission spectrum due to disintegration of water molecules in the plasma. In this work, a method that compares the experimentally obtained OH spectrum emitted from the steam plasma with the synthetic spectrum is used to determine the rotational temperature T_{rot} [30–32]. This method is very useful here especially with a spectrometer of relatively low spectral resolution. The theoretical diatomic molecular spectrum intensity is given by [33, 34]

$$I = D_0 k^4 S \exp\left(-\frac{E_r}{k_{\mathrm{B}} T_{\mathrm{rot}}}\right), \qquad (6)$$

where k is the wave number, S is the oscillator strength, k_{B} is the Boltzmann constant, D_0 is a coefficient containing the rotational partition function and E_r is the rotational energy level. The OH spectra are obtained from the data of Dieke and Crosswhite [34]. Note that instrumental broadening should be

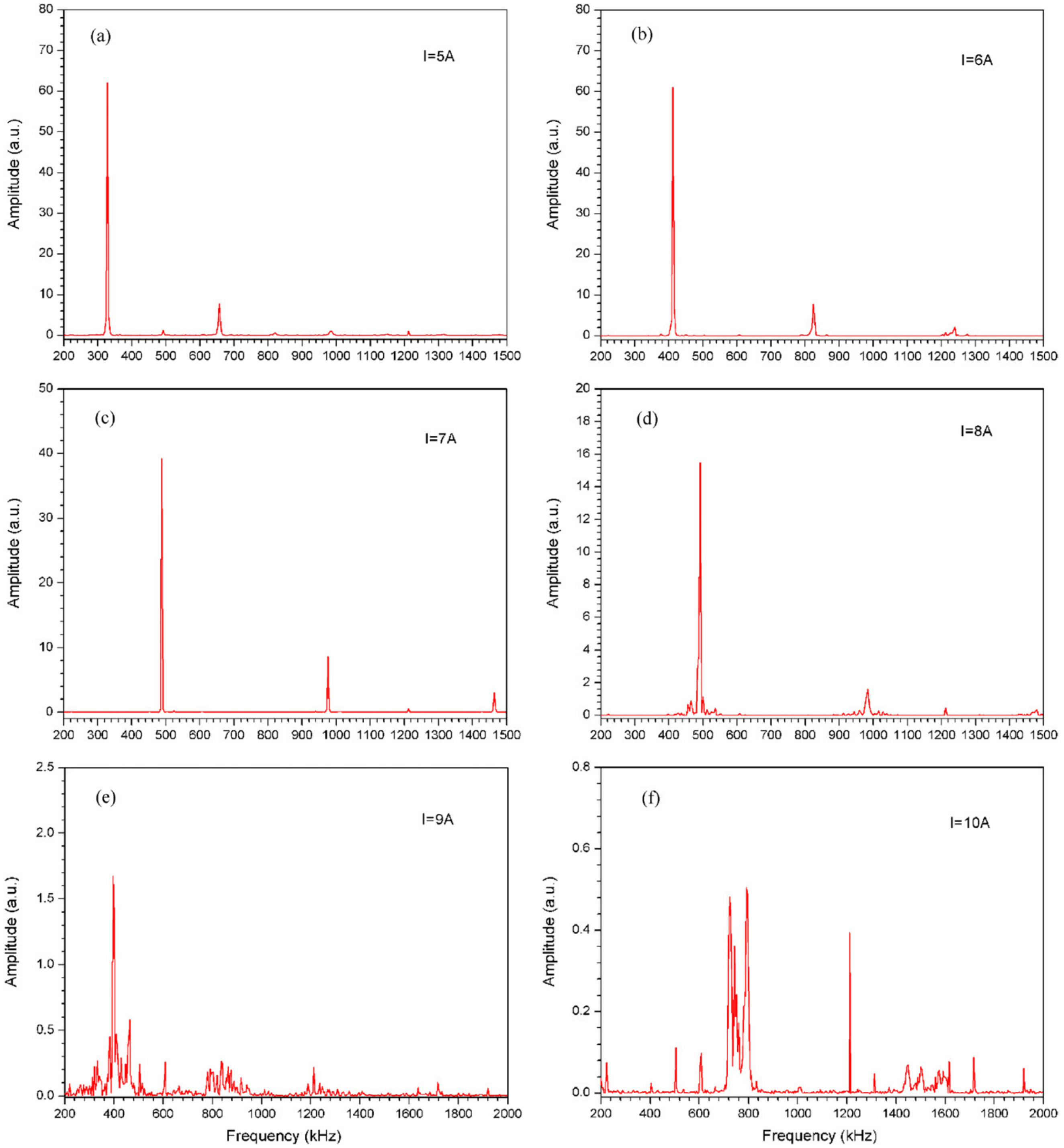

Figure 8. Voltage power spectra for currents (*a*) 5 A; (*b*) 6 A; (*c*) 7 A; (*d*) 8 A; (*e*) 9 A; (*f*) 10 A.

considered in the synthetic spectrum. Therefore, the synthetic intensity profile would be the convolution of equation (6) and the Gaussian shape (instrumental broadening), and is expressed as [35]

$$I = \frac{I_0}{\Delta_{\mathrm{i}}\sqrt{\pi/2}} \exp\left(-\frac{2(\lambda-\lambda_0)^2}{\Delta_{\mathrm{i}}^2}\right), \qquad (7)$$

where I_0 is the intensity obtained from equation (6) at wavelength λ_0, and Δ_{i} is the full-width at half-maximum (FWHM) of the instrumental broadening. On this basis, the synthetic spectra of OH are obtained through the summation of each line intensity in the wavelength region from 306 to 310 nm. Figure 10 presents a comparison of the experimental emission data (the open circular dots) with the profile of simulated optical emissions of OH spectrum at 5300 K represented by a solid curve, which shows good agreement. The same method is applied to calculate the gas temperature along the axis of the steam plasma jet at atmospheric pressure, and the results are shown in figure 11, under the experimental condition of dc power 1.04 kW (7 A, 150 V). The temperatures

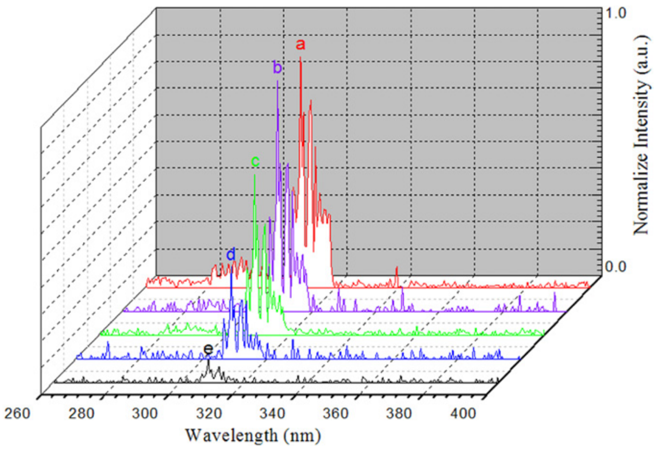

Figure 9. OH spectrum of the steam plasma jet on the axis at different positions ($a = 0$, $b = 5$, $c = 15$, $d = 20$ and $d = 25$ mm) from the nozzle exit.

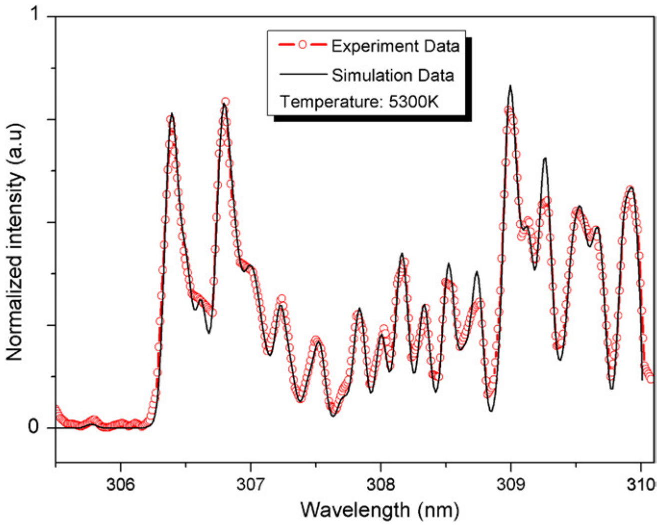

Figure 10. Profile of simulated optical emission of OH radicals (represented by the solid curve) in comparison with the experimental emission data (open circular dots), estimating the gas temperature to be $T = 5300$ K.

($T \leqslant 1500$ K) were also measured by a thermocouple, and the results were in agreement with those measured by OES.

3.4.2. Excitation temperature. The excitation temperature (T_{exc}) is a measure of the excitation capacity of atoms within the plasma, the Boltzmann plot method being the popular one used to obtain this temperature, because this method does not require a standard source for calibration. However, in order to increase the accuracy, a maximum energy area must be covered. The following equation is the expression of the Boltzmann plot method:

$$\ln\left(\frac{I_{ki}\lambda_{ki}}{g_k A_{ki}}\right) = \ln K - \frac{E_k}{k_{\mathrm{B}} T_{\mathrm{exc}}}, \qquad (8)$$

where I_{ki} is the line intensity, λ_{ki} is wavelength, g_k is the statistical weight of the upper atomic state, A_{ki} is the transition probability, E_k is the excitation energy, k_{B} is the Boltzmann constant and K is a constant for all the considered lines. Then, the slope of the straight line obtained is inversely proportional to the excitation temperature (T_{exc}).

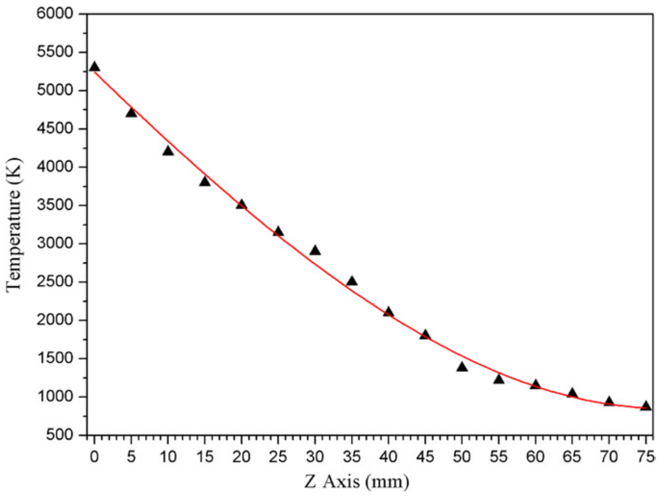

Figure 11. Axial distribution of gas temperature of the steam plasma jet at atmospheric pressure.

Table 1. Spectroscopic data of the hydrogen Balmer series.

Peak	λ (nm)	E_{ki} (eV)	Transition	$g_k A_{ki}$ (10^8 s^{-1})	Ref
H_α	656.28	1.889	3p → 2s	4.4101e − 01	NIST
H_β	486.13	2.550	4p → 2s	8.4193e − 02	NIST
H_γ	434.04	2.856	5p → 2s	2.5304e − 02	NIST
H_δ	410.18	3.022	6p → 2s	9.7320e − 03	NIST

From the Balemer series, the first four lines were observed with sufficient clarity ($H_\alpha, H_\beta, H_\gamma, H_\delta$) at the exit of the nozzle. The fifth line of this series was also observed, but not always with good resolution. Therefore, these lines are chosen to draw the Boltzmann diagram and derive the excitation temperature. The spectroscopic parameters of the selected lines taken from the atomic database of NIST [36] are shown in table 1.

Here, we cannot obtain the radial evolution of the electron temperatures of the plasma jet, because it is impossible to apply Abel inversion in the presence of the spectroscopic diagnostic set-up in our experiment and the plasma jet is actually very thin. Therefore, the plasma emission collected and transmitted by the optical fiber results from the integration of the spectral intensity along the line of sight. The calculated temperature in this case can be considered as that of the hottest zone of the plasma flow [37].

The typical Boltzmann plots obtained with the selected Balmer series lines is illustrated in figures 12(*a*)–(*c*). The excitation temperatures in the plasma central region are calculated to be 5700 ± 400 K at the torch exit ($z = 0$ mm), 5300 ± 300 K at the axial position of $z = 10$ mm and 4900 ± 300 K at the axial position of $z = 20$ mm, respectively. The weak axial gradient of the excitation temperatures can be seen in figure 12(*d*), which indicates the weak decay of plasma excitation in the steam plasma jet.

3.4.3. Electron number density. Stark broadening of spectral lines is a typical tool to determine the plasma electron density.

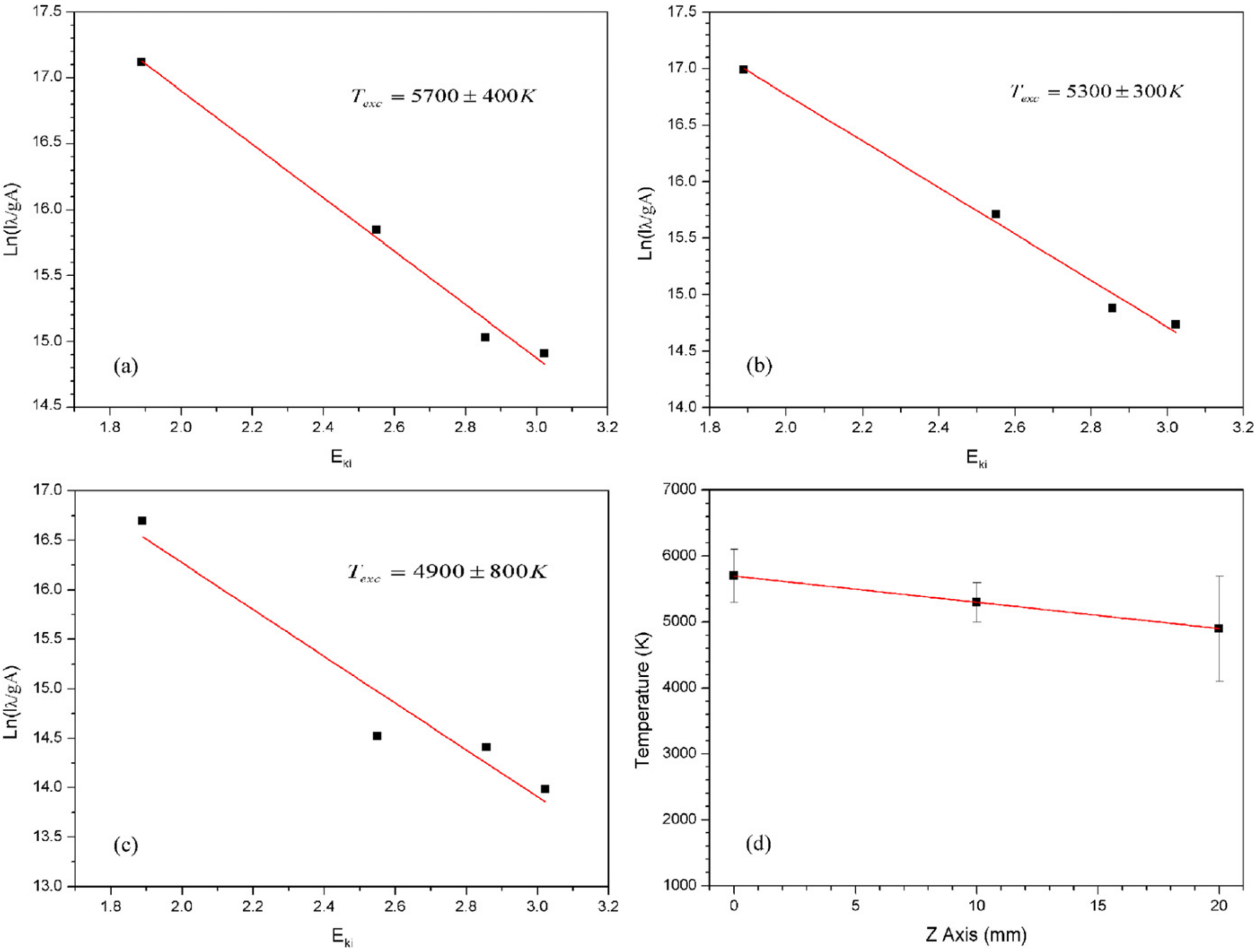

Figure 12. Typical Boltzmann plots for the selected hydrogen Balmer series lines at (*a*) $Z = 0$ mm; (*b*) $Z = 10$ mm; (*c*) $Z = 20$ mm; (*d*) axial distribution of excitation temperature of the steam plasma jet at atmospheric pressure.

Although the H_α line has the highest intensity among the hydrogen Balmer series in the steam plasma jet, it is not used to measure the electron densities in our study because of its sensitivity to self-absorption and strong broadening by ion dynamics [38, 39]. Stark broadening of the H_β Balmer line is used to deduce this value in our experiment, due to the immunity of its FWHM to ion dynamics effect and to temperature changes. Many researchers [39–41] have theoretically investigated this method many times, and given the following fit to obtain the plasma electron density from the FWHM without considering either the temperature or the perturber masses:

$$\mathrm{FWHM} = 4.8\,\mathrm{nm} \times \left(\frac{N_\mathrm{e}}{10^{23}\,\mathrm{m}^{-3}}\right)^{0.68116}. \tag{9}$$

Spectral line broadening is a complicated function of the environment of the radiating atoms or ions. The lineshape of the H_β transition is determined by the Lorentzian profile (Stark, van der Waals, resonance, natural) and the Gaussian one (Doppler and instrumental), broadening mechanisms that result in a Voigt profile. The Lorentzian half-width at half-maximum (HWHM) is the sum of the Lorentzian HWHMs, which can be expressed as

$$\Delta\lambda^{\beta}_{\mathrm{Lorentzian}} = \Delta\lambda^{\beta}_{\mathrm{Stark}} + \Delta\lambda^{\beta}_{\mathrm{Waals}} + \Delta\lambda^{\beta}_{\mathrm{Resonance}} + \Delta\lambda^{\beta}_{\mathrm{Natural}}. \tag{10}$$

The Gaussian HWHM is the square root of the sum of the squared Gaussian HWHMs, which can be expressed as

$$\Delta\lambda^{\beta}_{\mathrm{Gaussian}} = [(\Delta\lambda^{\beta}_{\mathrm{Doppler}})^2 + (\Delta\lambda^{\beta}_{\mathrm{Instrument}})^2]^{1/2}. \tag{11}$$

Under our operating conditions, the shape of the emission line and frequency shift come mainly from gas pressure and thermal motion of charged particles. So the natural broadening and resonance broadening can generally be ignored. The whole broadening attained by the profiles of H_β lines is the result of two Lorentzian broadenings, the Stark (λ_{Stark}) and van der Waals (λ_{Waals}) ones, and two Gaussian broadenings, the Doppler ($\lambda_{\mathrm{Doppler}}$) and the instrumental ($\lambda_{\mathrm{Instrument}}$).

The van der Waals broadening contributing to the Lorentzian FWHM of the H_β line is estimated as

$$\Delta\lambda^{\beta}_{\mathrm{Waals}} = \frac{4.10}{T_{\mathrm{g}}^{0.7}}\,\mathrm{nm}, \tag{12}$$

and is taken into account. As the van der Waals broadening depends on the perturbing molecule, the coefficient 4.10 in the

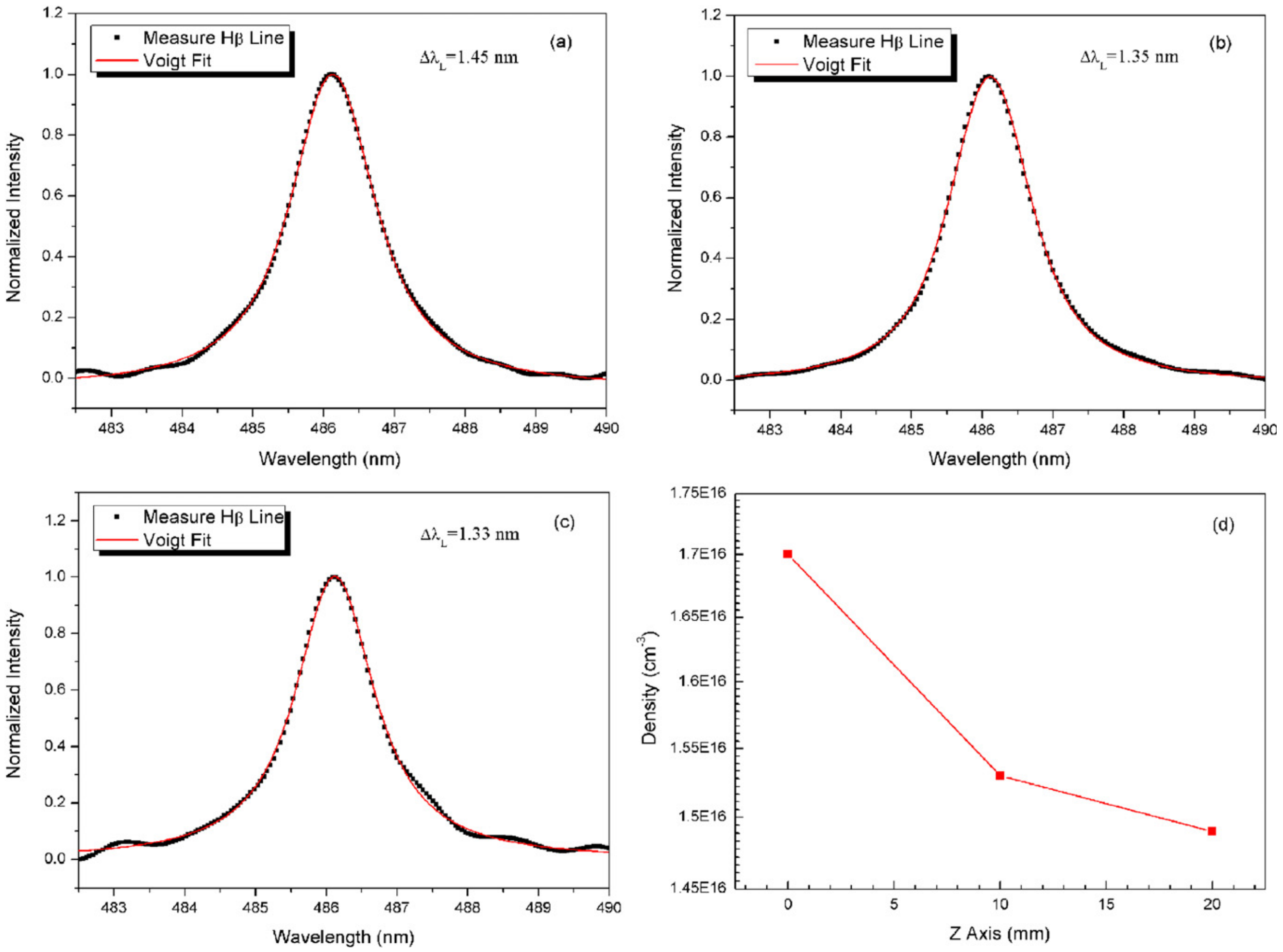

Figure 13. Typical Voigt fit of the recorded H_β line at (*a*) $Z = 0$ mm; (*b*) $Z = 10$ mm; (*c*) $Z = 20$ mm; (*d*) axial distribution of electron density of the steam plasma jet at atmospheric pressure.

former equation is introduced from [38], whose calculation result for water vapor is similar to our experiment. T_g is the gas temperature, which can be obtained from the rotational temperature of OH as before. Doppler broadening is caused by the random thermal motion of the emitting atoms and the FWHM of the H_β line is calculated by [42]

$$\Delta\lambda^{\beta}_{\mathrm{Doppler}} = 3.48 \times 10^{-4} T_g^{1/2}\ \mathrm{nm}. \qquad (13)$$

Instrumental broadening was determined using a low-pressure Hg–Cd lamp ($\Delta\lambda^{\beta}_{\mathrm{Instrument}} = 0.1$ nm).

In order to obtain the Lorentzian (Stark) part, a deconvolution recorded spectral line (fitting by Voigt function) is taken using the following relationship [42]:

$$\Delta\lambda_{\mathrm{Voigt}} \approx \left[\left(\frac{\Delta\lambda^{\beta}_{\mathrm{Lorentz}}}{2}\right)^2 + (\Delta\lambda^{\beta}_{\mathrm{Gauss}})^2\right]^{1/2} + \left(\frac{\Delta\lambda^{\beta}_{\mathrm{Lorentz}}}{2}\right). \qquad (14)$$

The recorded H_β line profiles at axial positions of $z = 0$ mm, 10 mm and 20 mm fitted with the Voigt function are shown in figures 13(*a*), (*b*) and (*c*), respectively. Therefore, the electron number density can be calculated using the above formulae. The results show that the electron number density also exhibits a slightly reducing trend along the jet axis, decreasing from $1.70 \times 10^{16}\ \mathrm{cm}^{-3}$ at the axial position of $z = 0$ mm, and $1.53 \times 10^{16}\ \mathrm{cm}^{-3}$ at the axial position of $z = 10$ mm to $1.49 \times 10^{16}\ \mathrm{cm}^{-3}$ at the axial position of $z = 20$ mm. These values are slightly higher than the LTE electron number density for the measured gas temperature of about 6000 K, which can be calculated by the Saha equation. This can be interpreted due to the high pressure at the axial center of the plasma jet and the high electrode erosion rates in the water plasma. Although the plasma jet is operated at atmospheric pressure, in essence, the pressure of the plasma jet center region is actually greater than atmospheric pressure, which results in the fact that the measured values will be greater than the calculated ones by the model of atmospheric pressure [43]. Furthermore, high erosion of copper electrodes (both cathode and anode) was observed as a result of electrode surface fusion by the action of the arc spot and high activity of the water plasma, which was also confirmed by the fact that strong emission lines of excited Cu were observed by OES. Large quantities of excited Cu were ionized in the steam thermal plasma, which resulted in an increase in the measured electron densities [44].

3.4.4. Local thermodynamic equilibrium. Minimum electron density is one of the most important standards to judge

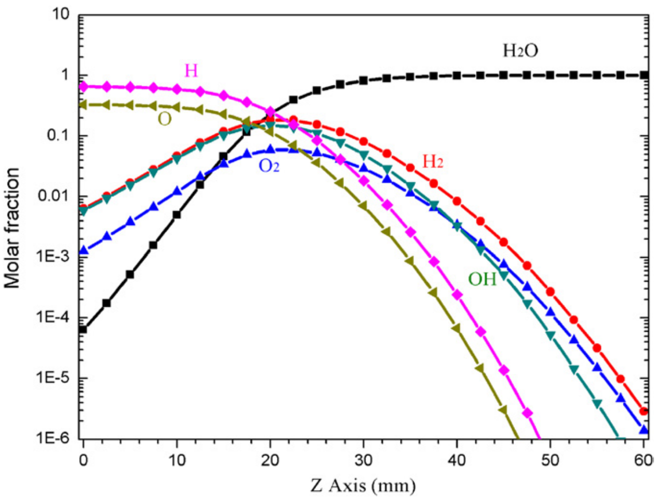

Figure 14. Axial distribution of composition of the steam plasma jet at atmospheric pressure.

whether the plasma is in LTE [45–52]. Based on his previous study, Griem revised the threshold value of electron density for the LTE state by considering the self-absorption of resonance radiation, and gave the following expression [45, 46]:

$$n_e \geqslant 1 \times 10^{17} \left(\frac{k_B T}{E_H}\right)^{\frac{1}{2}} \left(\frac{E_2 - E_1}{E_H}\right) (\text{cm}^{-3}). \qquad (15)$$

Assuming an electron temperature of 6000 K in the steam plasma jet, the minimum value of n_e obtained by equation (15) for LTE is 8.2×10^{15} cm^{-3}. Therefore, the electron densities in the steam plasma jet (at least in the axial range of 20 mm from the nozzle exit) can be considered to satisfy the LTE state.

3.4.5. Distribution of chemical composition in the steam plasma jet. One of the most significant differences from other inert gas plasmas is that water plasmas have many active species. Therefore, the concentrations of active species of water plasmas are one of the most important parameters, which contribute to its performance during application in the field of environment, such as organic wastewater decomposition. Herein, the chemical composition in the plasma jet is estimated under the assumption of LTE. Figure 14 depicts the molar fractions of species versus distance *Z* from the nozzle exit, which is estimated by minimization of Gibbs free energy, Dalton's law of partial pressures and the axis of temperature distribution of the plasma jet. The results show that H_2O molecules dissociated mainly into H, O, H_2, O_2 and OH radicals, and their axial distribution in the plasma jet is also shown. Moreover, as can be seen from figure 14, at an axial distance of 20 mm of the plasma jet, the molar fractions of these species in the steam plasma jet decreased sharply.

4. Conclusion

This work is devoted to the study of the characterization of an atmospheric steam plasma jet generated by a novel dc water plasma torch. Such an original configuration has been proven to be effective on improving the thermal efficiency. Through measurement of energy loss due to the heat loss of anode and cooling water for the torch body, the thermal efficiency of the torch is found to reach 90%, which is much higher than that of a normal gas-stabilized non-transferred plasma torch. Moreover, a high enthalpy is also demonstrated for the water plasma in our experiment, whose specific enthalpy is approximately (18.7 ± 1) MJ kg^{-1}.

The operational features of the torch are studied by analyzing the arc voltage, current and steam pressure signal. The water phase process for the initial operation of the torch involves a change from the liquid to the plasma state. Heat generated by the plasma arc converts liquid water into steam to serve as the plasma-forming gas, and hence three phases, liquid, gas and plasma, co-exist in the plasma source with a compact structure. Through a series of positive feedback effect, thermal equilibrium is established in the plasma source and the torch attains a relatively stable working state.

From the arc voltage trace analysis, restrike is identified as the main reason for the fluctuation of the steam plasma jet. Moreover, with the arc current increased, the frequency of fluctuation increases, while the amplitudes decrease. When the torch operates at a high current, intensified turbulence of the plasma jet makes the restrikes much more complicated. Several types of restrikes play important roles in the fluctuation of the steam plasma jet.

The parameters of the water plasma are determined by optical emission spectroscopy using various methods. In this work, the gas temperature along the plasma jet axis is determined by comparing the experimental emission data with the profile of simulated optical emissions of the OH spectrum. The highest temperature in the plasma jet is approximately 5300 K at the nozzle exit. In addition, the gas temperature along the jet axis drastically decreased to below 1000 K at a distance of approximately 75 mm. The hydrogen Balmer series lines are used to calculate the excitation temperature, which is approximately 5700 K at the nozzle exit, found using the Boltzmann plot method. The electron number density is derived from the Stark broadening of H_β, which reaches about 1.70×10^{-16} cm^{-3} at the nozzle exit. Along the axial distribution of the plasma jet, the measurements show that both excitation temperatures and electron number densities have weak axial gradient.

The steam plasma jet is demonstrated to be close to the LTE state by comparing the measured electron density with the threshold value of electron density for the LTE state. In addition, the axial distributions of the compositions of reactive species in the steam plasma jet are investigated based on the assumption of LTE. The results show that the main components of radicals in the steam plasma jet are H, O, H_2, O_2 and OH. Moreover, at an axial distance of 20 mm of the plasma jet, the molar fractions of these species in the steam plasma jet decreased sharply.

Acknowledgments

This study was supported by the National Natural Science Foundation of China (21171169) and the Knowledge Innovation Program of the Chinese Academy of Sciences.

References

[1] Kogelschatz U 2004 *Plasma Phys. Control. Fusion* **46** B63–75

[2] Bai Y, Han Z H, Li H Q, Xu C, Xu Y L, Wang Z, Ding C H and Yang J F 2011 *Appl. Surf. Sci.* **257** 7210–6

[3] Datye A, Koneti S, Gomes G, Wu K H and Lin H T 2010 *Ceram. Int.* **36** 1517–22

[4] Shimada S, Fuji Y, Kiyono H, Tsujino J and Yamazaki I 2009 *J. Ceram. Soc. Japan* **117** 415–20

[5] Jayasankar K, Samal S and Bhattacharjee S 2009 *High Temp. Mater. Process.* **13** 335–48

[6] Kim H I and Park D W 2004 *J. Indust. Eng. Chem.* **10** 234–8

[7] Zhao P, Ni G H, Jiang Y M, Chen L W, Chen M Z and Meng Y D 2010 *J. Hazard. Mater.* **181** 580–5

[8] Sakai S and Hiraoka M 2000 *Waste Manage.* **20** 249–58

[9] He X J, Ma T C, Qiu J S, Sun T J, Zhao Z B, Zhou Y and Zhang J L 2004 *Plasma Sources Sci. Technol.* **13** 446–53

[10] Huang H and Tang L 2007 *Energy Convers. Manage.* **48** 1331–7

[11] Rutberg P G 2003 *Plasma Phys. Control. Fusion* **45** 957–69

[12] Lemmens B, Elslander H, Vanderreydt I, Peys K, Diels L, Oosterlinck M and Joos M 2007 *Waste Manage.* **27** 1562–9

[13] Min B Y, Kang Y, Song P S, Choi W K, Jung C H and Oh W Z 2007 *J. Indust. Eng. Chem.* **13** 57–64

[14] Murphy A B, Farmer A J D, Horrigan E C and Mcallister T 2002 *Plasma Chem. Plasma Process.* **22** 371–85

[15] Tendler M, Rutberg P and van Oost G 2005 *Plasma Phys. Control. Fusion* **47** A219–30

[16] Kim S W, Park H S and Kim H J 2003 *Vacuum* **70** 59–66

[17] Nishikawa H, Ibe M, Tanaka M, Takemoto T and Ushio M 2006 *Vacuum* **80** 1311–5

[18] Jeništa J 1999 *J. Phys. D: Appl. Phys.* **32** 2763–76

[19] Ni G H, Meng Y D, Cheng C and Lan Y 2010 *Chin. Phys. Lett.* **27** 055203

[20] Bao S C, Guo W K, Ye M Y, Xu P and Zhang X D 2008 *Plasma Sci. Technol.* **10** 701–5

[21] Pfender E and Chang C H 1998 *Proc. 15th Int. Thermal Spray Conf. (Nice, France)* pp 315–27

[22] Ghorui S, Sahasrabudh S H, Murthy P S S, Das A K and Venkatramani N 2000 *IEEE Trans. Plasma. Sci.* **28** 253–60

[23] Hlina J 1989 *J. Phys. E: Sci. Instrum.* **22** 623–6

[24] Russ S, Pfender E and Strykowski P J 1994 *Plasma Chem. Plasma Process.* **14** 425–36

[25] Coudert J F, Planche M P and Fauchais P 1996 *Plasma Chem. Plasma Process.* **16** S211–27

[26] Singh N, Razafinimanana M and Hlina J 2000 *J. Phys. D: Appl. Phys.* **33** 270–4

[27] Duan Z, Wittmann K, Heberlein J, Coudert J F and Fauchais P 1999 *IEEE 26th Int. Conf. on Plasma Science (Monterey, CA, 20–24 June 1999)*

[28] Singh N, Razafinimanana M and Hlina J 2000 *J. Phys. D: Appl. Phys.* **33** 270–4

[29] Pauvit R, de Izarra C and Vallee O 1997 *High Temp. Mater. Process.* **1** 219

[30] Pellerin S, Cormier J M, Richard F, Musiol K and Chapelle J 1996 *J. Phys. D: Appl. Phys.* **29** 726–39

[31] de Izarra C 2000 *J. Phys. D: Appl. Phys.* **33** 1697–704

[32] Motret O, Hibert C, Pellerin S and Pouvesle J M 2000 *J. Phys. D: Appl. Phys.* **33** 1493–8

[33] Boumans P W J M 1987 *Inductively Coupled Plasma Emission Spectroscopy* Part 2 (New York: Wiley) chapter 10

[34] Dieke G H and Crosswhite H M 1962 T *J. Quant. Spectrosc. Radiat. Transfer* **2** 97–199

[35] Moon S Y and Choe W 2003 *Spectrochim. Acta* B **58** 249–57

[36] NIST Atomic Spectra Database Data, http://physics.Nist.gov/

[37] Tu X, Chéron B G, Yan J H and Cen K F 2007 *Plasma Sources Sci. Technol.* **16** 803–12

[38] Gigosos M A and Cardeñoso V 1987 *J. Phys. B: At. Mol. Opt. Phys.* **20** 6005–19

[39] Kelleher D E, Wiese W L, Helbig V, Greene R L and Oza D H 1993 *Phys. Scr.* **T47** 75–9

[40] Gigosos M A, González M Á and Cardeñoso V 2003 *Spectrochim. Acta* B **58** 1489–504

[41] Wiese W L, Kelleher D E and Helbig V 1975 *Phys. Rev.* A **11** 1854–64

[42] Bruggeman P, Schram D, González M Á, Rego R, Kong M G and Leys C 2009 *Plasma Sources Sci. Technol.* **18** 025017

[43] Burakov V S, Nevar E A, Nedel'ko M I, Savastenko N A and Tarasenko N V 2009 *J. Appl. Spectrosc.* **76** 856–63

[44] Auvrecht V, Bartlova M and Coufal O 2010 *J. Phys. D: Appl. Phys.* **43** 434007

[45] Griem H R 1963 *Phys. Rev.* **131** 1170

[46] Griem H R 1964 *Plasma Spectroscopy* (New York: McGraw-Hill)

[47] Richter J 1965 *Z Astrophysik* **61** 57

[48] Biberman L M, Vorobev V S and Lagarkov A N 1965 *Opt. Spectrosc. (USSR)* **19** 326

[49] Kolesnikov V N 1966 *Phys. Opt.* **30** 53

[50] Drawin H W 1969 *Z. Naturf.* a **24** 1492

[51] Drawin H W 1970 *High Pressure–High Temp.* **2** 359

[52] Novak J P 1976 *J. Quant. Spectrosc. Radiat. Transfer* **17** 247